

Interferometric observations of the Mira star α Ceti with the VLTI/VINCI instrument in the near-infrared



T. Driebe⁽¹⁾, C. Woodruff^(1,5), M. Eberhardt⁽¹⁾, K.-H. Hofmann⁽¹⁾, K. Ohnaka⁽¹⁾, A. Richichi⁽²⁾, D. Schertl⁽¹⁾, M. Schöller⁽³⁾, M. Scholz^(4,5), G. Weigelt⁽¹⁾, M. Wittkowski⁽²⁾, and P. R. Wood⁽⁶⁾

(1) Max-Planck-Institut für Radioastronomie, Bonn, (2) European Southern Observatory, Garching, (3) European Southern Observatory, Santiago, (4) Institut für Theoretische Astrophysik der Univ. Heidelberg, (5) Institute of Astronomy, Univ. of Sydney, (6) Research School of Astronomy and Astrophysics, Weston Creek



MAX-PLANCK-GESellschaft

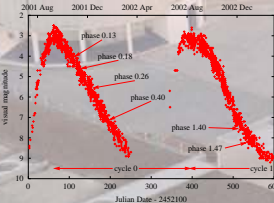
Abstract

We present K-band commissioning observations of the Mira star prototype α Ceti obtained at the ESO Very Large Telescope Interferometer (VLTI) with the VLT Interferometer Commissioning Instrument (VINCI) and two siderostats. The observations were carried out between 2001 October and December, in 2002 January and December, and in 2003 January. Rosseland angular radii are derived from the measured visibilities by fitting theoretical visibility functions obtained from center-to-limb intensity variations (CLVs) of Mira star models. Using the derived Rosseland angular radii and the spectral energy distributions (SEDs) reconstructed from available photometric and spectrophotometric data, we find effective temperatures ranging from $T_{\text{eff}} = 3192 \pm 200$ K at phase $\Phi = 0.13$ to 2918 ± 183 K at $\Phi = 0.26$. Comparison of these Rosseland radii, effective temperatures, and the shape of the observed visibility functions with model predictions suggests that α Ceti is a fundamental mode pulsator. Furthermore, we investigated the variation of visibility function and diameter with phase. The Rosseland angular diameter of α Ceti increased from 28.9 ± 0.3 mas (corresponding to a Rosseland radius of $332 \pm 38 R_{\odot}$ for a distance of $D = 107 \pm 12$ pc) at $\Phi = 0.13$ to 34.9 ± 0.4 mas ($402 \pm 46 R_{\odot}$) at $\Phi = 0.4$. The observational error of the Rosseland linear radius almost entirely results from the error of the parallax, since the error of the angular diameter is only approximately 1%.

Introduction

Mira stars are long-period variables which evolve along the asymptotic giant branch (AGB) with well-defined pulsation periods (80-1000 days). Because of their large visual light curve amplitudes, they are easily identified and classified. Fig. 1 shows the visual light curve of α Ceti together with the dates at which the VINCI observations were carried out. The change of CLV and spectral type with phase and cycle, as well as the brief time these stars remain in the variable stage, pose interesting problems for observation and modeling.

Figure 1: Visual light curve for α Ceti between JD 2452100 and 2452700. The VINCI visibilities were measured at the following phases: $\Phi = 0.13$ (2001 Oct 22/23), $\Phi = 0.18$ (2001 Nov 09/15/17), $\Phi = 0.26$ (2001 Dec 06), $\Phi = 0.40$ (2002 Jan 20), $\Phi = 1.40$ (2002 Dec 20), and $\Phi = 1.47$ (2003 Jan 09).



Observations

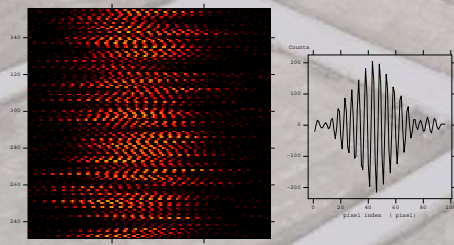


Figure 2: Interferometric fringes obtained with VINCI. *Left:* Interferograms for α Ceti with a baseline of 16 m. The y-axis shows the interferogram number, and each horizontal line corresponds to an individual interferogram (pseudocolor). These interferograms are produced by modulating the optical path difference (OPD) via a mirror mounted on a piezo translator. *Right:* Single interferogram (no. 223). The y-axis is given in arbitrary units of relative intensity. In both panels the x-axis gives the pixel number which is a measure of the OPD.

Date	JD	cycle+ Φ	N	B_p [m]	P.A. [°]
2001 Oct 22	2452205	0.13	13	11.5 - 16.0	62-73
2001 Oct 23	2452206	0.13	12	11.5 - 16.0	63-73
2001 Nov 09	2452223	0.18	6	14.5 - 16.0	71-73
2001 Nov 15	2452229	0.18	3	15.5 - 16.0	72-73
2001 Nov 17	2452231	0.18	3	14.5 - 15.0	70
2001 Dec 06	2452250	0.26	6	15.0 - 16.0	72-73
2002 Jan 20	2452295	0.40	2	14.0 - 14.5	72
2002 Dec 20	2452629	1.40	2	7.5 - 8.0	73-74
2003 Jan 09	2452649	1.47	1	8.0	73

Tab. 1: Summary of VINCI commissioning observations of α Ceti. Date, Julian Date JD, cycle and visual phase Φ , number of visibility data points N , projected baseline length B_p , and baseline projection angle P.A.

Although VINCI was designed only for the VLTI commissioning program, it provided enough scientific data to allow investigations of several southern Mira stars, many of them being first-time visibility determinations. α Ceti is an ideal target for infrared interferometry because of its large photospheric size and its relatively small distance from Earth (HIPPARCOS: 107 pc) together with a substantial infrared flux. Parameters of the VINCI measurements of α Ceti are summarized in Tab. 1.

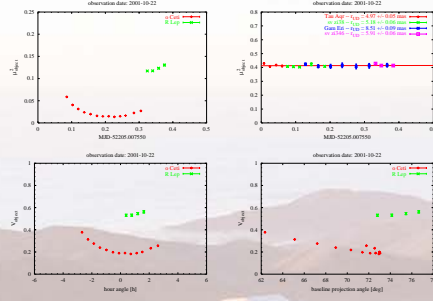


Figure 3: *Top left:* Uncalibrated visibilities of α Ceti and another Mira star, R Lep, plotted vs. modified Julian date (MJD). The curved shape of the visibilities arises from the change of the projected baseline length caused by the Earth's rotation. *Top right:* Linearly fitted transfer function (i.e. measure of the instrument's fringe contrast loss) obtained from calibrator stars measured during the same night. The transfer function is used to calibrate the raw object visibilities. *Bottom left:* Calibrated visibilities of the objects α Ceti and R Lep plotted vs. hour angle. *Bottom right:* Calibrated visibilities plotted vs. baseline projection angle (PBA). The PBA change of less than 10° does not allow for a detailed study of asymmetries.

Diameter-phase relationship

After the reduction and analysis of the data, all measurements were binned according to phase. The data for each phase bin were compared with theoretical calculations for Mira atmospheres from BSW, HSW, ISW, and TLSW. These models use non-linear pulsation models for both fundamental and first-overtone pulsation modes and exhibit characteristic cycle-to-cycle distinctions. Among the outputs, they produce light curves and synthetic spectra, as well as giving radius and effective temperature.

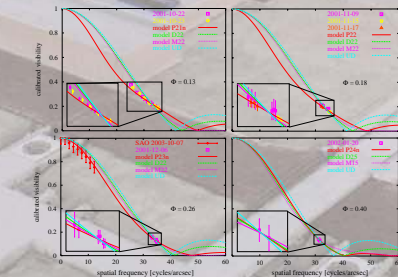


Figure 4: Visibilities vs. spatial frequency for α Ceti at four different phases (see labels). The insets show an enlargement of the relevant spatial frequency range. Here, the error bars are included. The solid lines show fits with different Mira star models: Solid lines represent the P models from TLSW and ISW, dashed lines the D models from BSW, dotted lines the M models from HSW, and the dash-dotted lines represent the simple uniform-disk model CLVs. For phase 0.26 (lower left panel), SAO speckle interferometry data measured at the same phase but at a different cycle (observation date 2003 Oct 07) are shown. These additional data have not been used for the fits, but they illustrate that there is no indication for a visibility contribution from a circumstellar dust shell at low spatial frequencies.

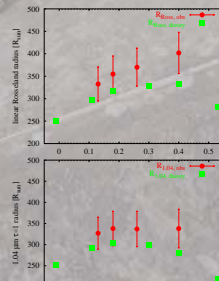


Fig. 5: *Top:* Linear Rosseland radii of α Ceti derived from P21n, P22, P23n, and P24n series models of ISW (filled circles) at four different phases ($\Phi = 0.13$: $R_{\text{Ross}} = 332 \pm 38 R_{\odot}$; $\Phi = 0.18$: $R_{\text{Ross}} = 354 \pm 41 R_{\odot}$; $\Phi = 0.26$: $R_{\text{Ross}} = 370 \pm 42 R_{\odot}$; $\Phi = 0.40$: $R_{\text{Ross}} = 402 \pm 46 R_{\odot}$) and theoretical P2r models (filled squares). The diagram clearly shows a monotonic increase of radius with decreasing brightness, in line with the predictions from TLSW. *Bottom:* Derived (filled circles) and theoretical (filled squares) $R_{1.01}$ radii (=continuum radii at $\lambda = 1.04 \mu\text{m}$) of α Ceti.

Center-to-Limb Variations

The visibilities measured for α Ceti at phase 0.13 (observation date: 22/23 Oct. 2001) are best fitted with the TLSW model P22. This particular model was calculated for α Ceti at phase 0.2 in the second cycle of computation. The P series fundamental mode models agree best with the measured visibilities and the derived radii, whereas the D series models do not represent Mira well. From the CLV fit of the visibility curve, together with HIPPARCOS measurements, a Rosseland radius of approximately $330 R_{\odot}$ was obtained. The accuracy of the fit for three models (P22, fully darkened disk and uniform disk), together with the shape of the model CLV, can be seen in Fig. 6. Although the measured visibility shapes are in good agreement with the predictions made by the TSW P models, we nevertheless want to point out that the observed visibility function might also arise from an asymmetric shape of the stellar disk or inhomogeneous surface structures such as giant convection cells.

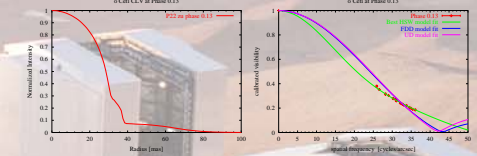


Figure 6: *Left:* CLV of the TLSW model P22 for α Ceti at phase 0.2. The intensity is normalized to 1 at the disk center, and the angular diameter is given in mas. The extended wing of the CLV is mainly caused by water molecules in the outer region of the atmosphere. *Right:* Visibility of α Ceti measured at phase 0.13. The green line denotes the model visibility curve derived from the intensity distribution shown in the left panel. As can be seen, the model visibility shape is in good agreement with the observations in the observed baseline range. The blue and purple lines show the visibility function derived from a fully darkened disk (FDD) and an uniform disk (UD) respectively.

Radii and effective temperatures

Angular stellar filter radii and Rosseland radii were derived from the measured visibilities by fitting theoretical center-to-limb intensity variations of different Mira star models to the observed visibilities. When available, HIPPARCOS parallaxes allowed us to determine linear radii. The bolometric flux was obtained by integration of the spectral energy distribution (SED) for α Ceti and two other Mira stars, R Lep and S Ori, at different phases. The effective temperature T_{eff} was derived from the Rosseland diameter and the bolometric flux. The results are summarized in Table 1.

	Φ	model	d /mas	R/R_{\odot}	T_{eff} /K	$R_{\text{model}}/R_{\odot}$	$T_{\text{eff,model}}/K$
α Ceti	0.13	P22	28.90 ± 0.3	332 ± 38	3192 ± 200	296	2640
R Lep	0.20	P22	15.20 ± 0.2	400 ± 90	2214 ± 180	318	2700
S Ori	0.80	P28	9.78 ± 0.2	-	2700 ± 240	190	3550

Table 1: Phases Φ , model used, angular Rosseland diameters d (derived by fitting P model visibilities to the observed visibilities), derived linear Rosseland radii R , effective temperature T_{eff} (derived by using P models), P model Rosseland radii R_{model} , and P model effective temperatures $T_{\text{eff,model}}$ for α Ceti, R Lep, and S Ori.

Conclusions

- Rosseland radius and effective temperature were determined for α Ceti and two other Mira stars (R Lep and S Ori, see Tab. 1) based on interferometric measurements with the VLTI/VINCI instrument in the K band.
- The Rosseland diameter of α Ceti increased from 28.9 ± 0.4 mas at phase $\Phi = 0.13$ to 34.9 ± 0.4 mas at phase $\Phi = 0.4$. The effective temperature decreased from $T_{\text{eff}} = 3192 \pm 200$ K at $\Phi = 0.13$ to 2918 ± 183 K at $\Phi = 0.26$.
- The visibility shape of the Mira star model P22 from TLSW is in good agreement with the measured visibilities in the observed baseline range.
- Comparison of the model Rosseland radius (model P22, $R = 318 R_{\odot}$) and derived Rosseland radius of α Ceti at ($R = 328 \pm 37 R_{\odot}$) at $\Phi = 0.13$ show good agreement.
- A more detailed discussion on the topics presented here is given in Woodruff et al. (2004).

References

Bessell, M.S., Scholz, M., & Wood, P.R. (BSW) 1996, *A&A* 307, 481
 Hofmann, K.-H., Scholz, M., & Wood, P.R. (HSW) 1998, *A&A* 339, 846
 Ireland, M.J., Scholz, M., & Wood, P.R. (ISW) 2004, *MNRAS* 352, 318
 Tej, A., Lincon, A., Scholz, M., & Wood, P.R. (TLSW) 2003, *A&A* 412, 481
 Woodruff, H.C., Eberhardt, M., Driebe, T., Hofmann, K.-H., Ohnaka, K., Richichi, A., Schertl, D., Schöller, M., Scholz, M., Weigelt, G., Wittkowski, M., Wood, P.R. 2004, *A&A* 421, 703

Poster presented at the ESO workshop
 The power of optical/IR interferometry: recent scientific results and 2nd generation VLTI instrumentation
 4th-8th April 2005, Garching, Germany
 contact e-mail: driebe@mpeifr-bonn.mpg.de